

Formation of high- β plasma and stable confinement of toroidal electron plasma in Ring Trap 1^{a)}

H. Saitoh,^{b)} Z. Yoshida, J. Morikawa, M. Furukawa, Y. Yano, Y. Kawai, M. Kobayashi, G. Vogel, and H. Mikami

Department of Advanced Energy, Graduate School of Frontier Sciences, University of Tokyo, 5-1-5 Kashiwanoha, Kashiwa, Chiba 277-8561, Japan

(Received 22 November 2010; accepted 11 February 2011; published online 11 April 2011)

Formation of high- β electron cyclotron resonance heating plasma and stable confinement of pure electron plasma have been realized in the Ring Trap 1 device, a magnetospheric configuration generated by a levitated dipole field magnet. The effects of coil levitation resulted in drastic improvements of the confinement properties, and the maximum local β value has exceeded 70%. Hot electrons are major component of electron populations, and its particle confinement time is 0.5 s. Plasma has a peaked density profile in strong field region [H. Saitoh *et al.*, 23rd IAEA Fusion Energy Conference EXC/9-4Rb (2010)]. In pure electron plasma experiment, inward particle diffusion is realized, and electrons are stably trapped for more than 300 s. When the plasma is in turbulent state during beam injection, plasma flow has a shear, which activates the diocotron (Kelvin–Helmholtz) instability. The canonical angular momentum of the particle is not conserved in this phase, realizing the radial diffusion of charged particles across closed magnetic surfaces. [Z. Yoshida *et al.*, Phys. Rev. Lett. **104**, 235004 (2010); H. Saitoh *et al.*, Phys. Plasmas **17**, 112111 (2010).]. © 2011 American Institute of Physics. [doi:10.1063/1.3567523]

I. INTRODUCTION

The Ring Trap 1 (RT-1) device¹ is a magnetospheric configuration generated by a levitated superconducting magnet.^{2–5} Interactions between the strongly inhomogeneous dipole field and charged particles produce diverse structures of plasmas.⁶ Dipole field is the most fundamental and widely observed magnetic configuration in the universe. The magnetospheric configuration enables novel laboratory experiments for understanding the fundamental properties of space plasmas as well as for a lot of scientific applications.

One of the examples of these plasma phenomena is high- β flowing plasma in the Jovian magnetosphere, which was discovered by spacecraft observations.⁷ Theoretically, effects of strong compressibility of flux tubes can explain the stability of high- β plasma even in the bad curvature region of the dipole field.^{8,9} Dynamic pressure of fast plasma flow can balance the thermal pressure of plasma, and ultra high- β state (possibly exceeding 100%) of flowing plasma is theoretically predicted¹⁰ as a new relaxation state of plasma.¹¹ High- β confinement in the magnetospheric configuration is attractive for fusion plasma studies because it can be applied for advanced fusion concept burning D-D⁹ and D-³He¹² fuels. Recently, magnetospheric configurations with superconducting dipole field magnets are constructed [RT-1 (Ref. 2) and Levitated Dipole Experiment (LDX) (Ref. 4)], and both of the groups have succeeded to stably confine high- β plasma in the dipole field configuration.

Another example of interesting behaviors of charged particles in the magnetospheric configuration is inward diffusion and self-organization of equilibrium.^{3,5,13} Instabilities activate

effective radial transport of particles until stable equilibrium state is spontaneously generated. Hasegawa⁸ pointed out that the self-organization of plasma is realized so that particle density per flux tube becomes constant. In the strongly inhomogeneous dipole field configuration, this constraint results in effective inward diffusion and peaked density profile in the strong field region. Inward pinch of particles is one of the key issues for particle injection process of toroidal non-neutral plasmas as well as for the formation of high temperature fusion plasma. In contrast to the widely used linear configurations for non-neutral plasma trap,¹⁴ toroidal geometries^{15–22} can trap charged particles independently of its electric signs.¹⁷ It can then in principle confine plasmas of arbitrary neutrality including multispecies antimatter particles.

In this study, we report the long time (up to 370 s) confinement of toroidal pure electron plasma^{3,23} and formation of high- β electron cyclotron resonance heating (ECH) plasma²⁴ in RT-1 including the review of recent experimental results. In the study of non-neutral plasma, measurements of internal structures and electrostatic fluctuation consistently showed that rigid-rotating stable equilibrium is spontaneously generated. We developed a nondestructive diagnostics method for spatial structures of non-neutral plasma in a toroidal geometry and found that the particles diffuse inward due to fluctuation-induced asymmetry of the trap system. In the experiment of ECH plasma, optimization of formation conditions and compensation of the geomagnetic field drastically improved the confinement properties, and local β exceeded 70%. Hot electrons generated by ECH are major component of electron populations, and particle confinement time $\tau_p \sim 0.5$ s. Density profiles estimated from multicord interferometry showed peaked distribution in the strong field region.

^{a)}Paper G13 5, Bull. Am. Phys. Soc. **55**, 110 (2010).

^{b)}Invited speaker.

II. THE RT-1 DEVICE

Figure 1 shows the cross sectional view and photographs of RT-1 (Ref. 2) and generated plasma. The research goals of RT-1 are to realize confinement of ultra high- β plasma suitable for burning advanced fusion fuels and to stably trap toroidal non-neutral plasmas including antimatter particles. Inside the vacuum chamber, RT-1 has a Bi-2223 high-temperature superconducting dipole field magnet.²⁵ The dipole field magnet is levitated in order to minimize perturbations to the plasma. The vertical position of the superconducting magnet is monitored by three laser sensors, and a levitation magnet, located at the top of the chamber, is feedback-controlled to realize stable coil levitation.²⁶ Combination of the superconducting magnet and the levitation magnet generates a magnetic separatrix configuration as shown in Fig. 1(a). Outside of the chamber, a set of geomagnetic field compensation coil is installed [Fig. 1(b)].²⁷ Neutral plasma is generated by ECH with 8.2 GHz (1 s, 25 kW) and 2.45 GHz (2 s, 20 kW) microwaves. Working gas was hydrogen and helium. Non-neutral plasma is generated by injecting electron beam from a LaB₆ cathode electron gun located at the edge of the confinement region. Detailed explanation of RT-1 is found in Ref. 2.

III. CONFINEMENT OF PURE ELECTRON PLASMA

A. Particle injection and stable confinement

Magnetospheric configuration generates an axially symmetric toroidal system that can confine plasmas of arbitrary

neutrality.¹⁷ The canonical angular momentum $P_\theta = mrv_\theta + qrA_\theta \sim qrA_\theta$ and the third adiabatic invariant $K \sim \int P_\theta ds \sim q\Phi$ of a charged particle are conserved in the axisymmetric system.¹⁴ Spatial deviation of a particle from its initial magnetic surface is then smaller than the poloidal Larmor radius, $d < |mr\dot{\theta}/qB_\theta|$. Strongly magnetized particles cannot travel across magnetic surfaces, and excellent confinement properties are expected for charged particles independently of its electric signs.

One of the difficult issues for the formation of toroidal non-neutral plasma is particle injection method.²⁸ Although particles may be stably trapped inside the toroidal closed magnetic surfaces, it must be injected from outside of the confinement region prior to the trapping phase. This is in strong contrast to the cases of linear non-neutral plasma traps,¹⁴ where particles can be injected and ejected along open field lines. In RT-1, effective radial particle transport is realized through fluctuation-induced violation of the trap symmetry.³ During beam injection, plasma has fluctuations that induce asymmetry of the system. In this phase, conservations of P_θ and K are temporally violated and it results in effective particle transport.

Figure 2 shows typical temporal evolutions of electrostatic fluctuation and its frequency power spectrum in the beam injection and stabilization phases. Electrons were injected from $t = 0$ to 0.1 s with an initial acceleration voltage of $V_{acc} = 140$ V. During beam injection, plasma has a large turbulentlike fluctuation, as shown in Fig. 2(c-1), and the trap symmetry is temporary violated. When the system is

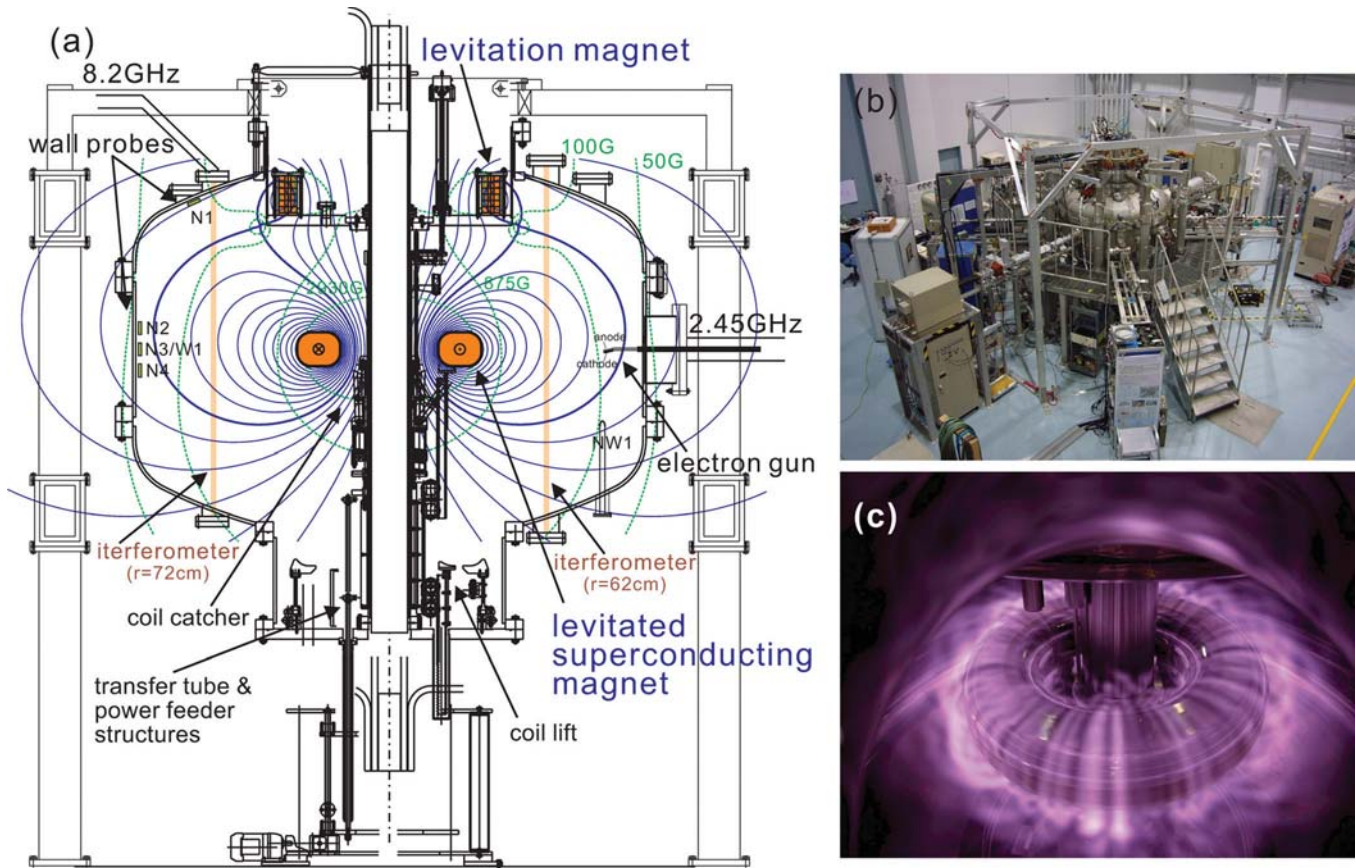


FIG. 1. (Color online) (a) R-z cross section, and photographs of (b) bird-eye view and (c) magnetospheric plasma in RT-1.

not symmetric, particles can be transported radially until the formation of stable equilibrium state. After injection ended at $t = 0.1$ s, rapid growth and decay of fluctuation amplitude were observed. In this phase, turbulence component of the fluctuation was gradually dumped [Figs. 2(c-2) and 2(c-3)]. At $t = 0.6$ s, plasma had quite peaked frequency spectrum as shown in Fig. 2(c-4). After this period, very stable state was realized.

Typical behaviors of fluctuation in longer period are shown in Fig. 3. Electrons were injected from $t = 0$ to 0.1 s. As shown in Fig. 3(a), stable state lasted for more than 300 s and ended with a rapid growth and decay of instability. Formation of ions due to collisions with neutral molecules and the resultant two stream effect is the possible reason for the onset of instability. Sometimes plasma is not stabilized after beam injection ends as shown in Fig. 3(b), and growth and decay of fluctuations are repeatedly observed. This unstable mode was observed especially when $V_{acc} > 200$ V. Stable confinement time and duration time of the electrostatic oscillation for the two modes are shown in Fig. 4. The trap time was significantly short when the plasma fails to enter the quiescent state, indicating the effects of fluctuation-induced rapid loss of electrons. The stable confinement time strongly depends on the neutral gas pressure P_n and was observed to be proportional to $P_n^{-0.35}$. It deviates from classical dependence of P_n^{-1} , also suggesting that the effects of ion formation rather than classical diffusion set the upper limit of the confinement time.

B. Internal structure and fluctuation properties

Measurements of density and space potential profiles consistently show that the toroidal $E \times B$ drift velocity of the plasma is close to rigid-rotating motion during beam injection, when the superconducting magnet is levitated.²³ Electrostatic fluctuation measurements show that the plasma fluctuation propagates in the toroidal electron diamagnetic direction. The electrostatic oscillations were simultaneously measured by using walls located at different poloidal and toroidal positions, and a rake Langmuir probe located at different radial positions. We found that the fluctuation has

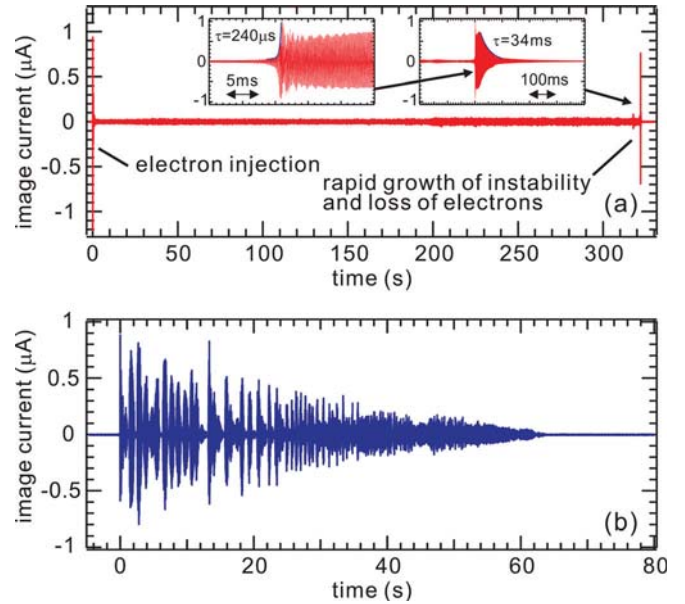


FIG. 3. (Color online) Typical temporal evolutions of electrostatic fluctuations (a) when the plasma is stabilized and long time confinement is realized (Ref. 23) and (b) when the plasma is not stabilized.

approximately same frequencies in the entire plasma region. Phase difference of the fluctuation was observed only in the toroidal direction. Toroidal separation angles between the wall probes agreed with the phase differences of the fundamental mode, indicating that the lowest toroidal mode number was $n = 1$.

The observed fluctuation frequency range was close to the toroidal $E \times B$ rotation frequency $f_{E \times B}$. By using a poloidal magnetic field strength $B = 10^{-2}$ T and radial electric field $E_r = 500$ V/m at $r = 0.8$ m, we have $f_{E \times B} = E / 2\pi r B \sim 10$ kHz, which shows a rough agreement with the observed fluctuation frequency range during the electron injection. Figure 5(a) shows the frequencies of the fundamental mode of the fluctuation in the variation of V_{acc} during the electron injection. The fluctuation frequency is proportional to V_{acc} . Because the shapes of potential profiles are similar for different V_{acc} , the frequency is approximately proportional to E_r . Although

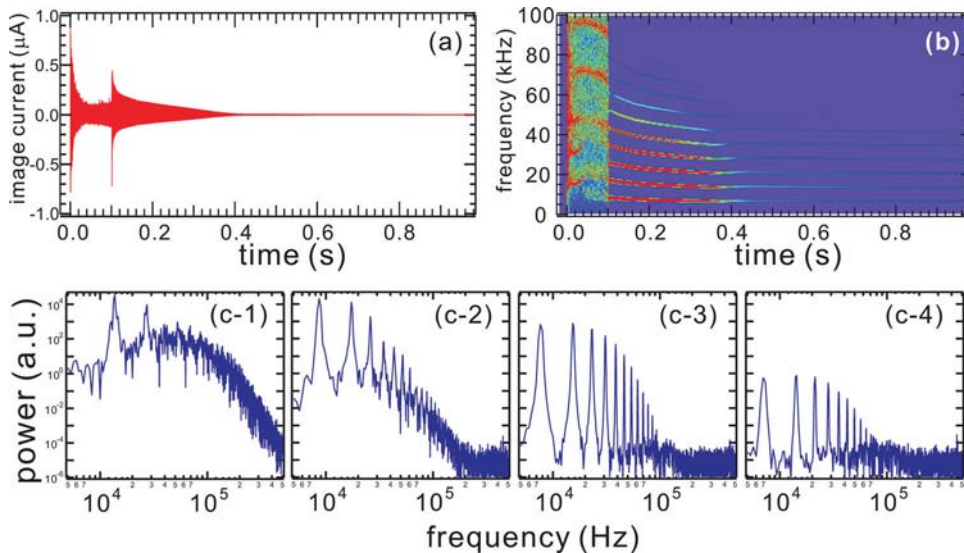


FIG. 2. (Color online) Temporal evolutions of (a) electrostatic fluctuation measured by a wall probe and (b) FFT spectrum of the fluctuation. Electrons were injected from $t = 0$ s to 0.1 s. (c) Frequency power spectrum at (1) $t = 0.01$ s, during beam injection, (2) $t = 0.11$ s, just after injection ended, (3) $t = 0.2$ s and (4) $t = 0.6$ s.

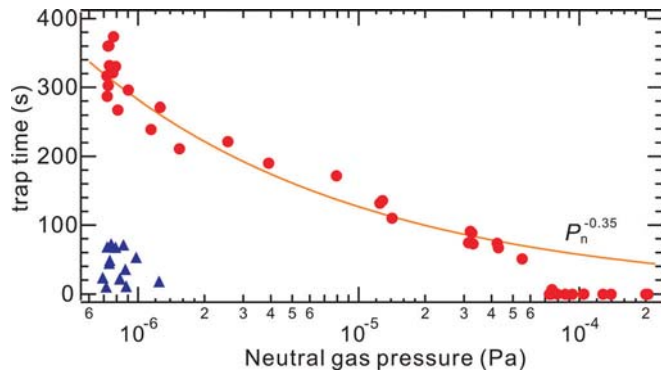


FIG. 4. (Color online) Confinement time in variation of neutral gas (hydrogen) pressure when stable confinement is realized [circles, correspond to the waveform of Fig. 3(a)] (Ref. 23) and not realized [triangles, correspond to Fig. 3(b)].

the magnetic field strength is fixed in RT-1, we changed the radial position of the electron gun and plotted the observed fluctuation frequency in Fig. 5(b). When the gun was located inside the magnetic separatrix ($r_{gun} < 92.5$ cm), the frequency was inversely proportional to B , field strength at the electron gun position. Propagation and frequency properties suggest that the observed fluctuation is the toroidal version of the diocotron (Kelvin–Helmholtz) mode in the magnetospheric configuration.

C. Inward diffusion of particles

Besides the particle injection method, another difficult issue concerning the toroidal non-neutral plasma is its diagnostics method. This is in contrast to the cases of linear traps again, where particles can be extracted along field lines and various information of plasmas can be measured.¹⁴ During beam injection, we can use Langmuir probes to directly measure the spatial structures of the electron plasma. However, probe insertion seriously perturbs the plasma and long time confinement is not realized. Properties of the plasma in the stable confinement phase are subjects of interest, and therefore nondestructive measurement method is strongly needed for toroidal non-neutral plasmas.

We estimate the spatial profiles of toroidal non-neutral plasma by using wall probes and current integration circuits.²⁹ If we can divide the whole plasma volume into m regions and the averaged electron density at each region is n_i ($i = 1 - m$), image charge Q_j ($j = 1 - m$) induced on each wall is given by

$$[Q_j]_{m \times 1} = [a_{ij}]_{m \times m} [n_i]_{m \times 1}, \quad (1)$$

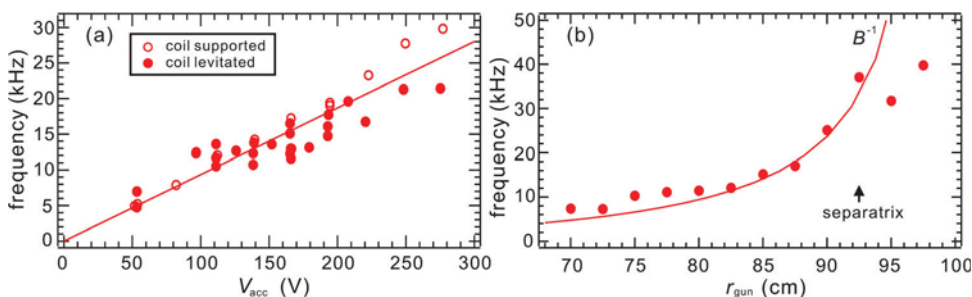


FIG. 5. (Color online) Frequencies of electrostatic fluctuation during electron injection (a) in variation of acceleration voltage of electron gun and (b) in variation of radial electron gun position.

where a_{ij} is a proportional constant of the image charge on a wall j induced by the plasma charges in region V_i . $A = [a_{ij}]$ is chosen so that the Poisson equation satisfies the boundary condition on the chamber wall. The electron density in each region is then given by

$$[n_i]_{m \times 1} = A^{-1} [Q_j]_{m \times 1}, \quad (2)$$

and detailed density profiles can be estimated by using a sufficient number of walls. Because the image current is measured by a current amplifier and the wall is electrically shorted to the chamber, the use of wall probe does not affect the potential structure of the plasma. Therefore, this method can be used for nondestructive measurement of the toroidal non-neutral plasma.

In this study, we used only three wall probes located at the same $r - z$ cross section of the device as shown in Fig. 1(a) as N2, N3, and N4,²⁹ and the spatial resolution of the measurements was not very high. We assume that the electron density has power-law dependence on r on the $z = 0$ plane

$$n(r) = n_0 r^{-a}, \quad (3)$$

and is constant on magnetic surfaces. Note that the wall probes were located at the chamber wall at $r = 100$ cm, so they are not sensitive to the charges near the superconducting coil. When a in Eq. (3) is small and the plasma has a large volume, its surface is close to the chamber wall. Then the profiles of image charge σ_i on the chamber wall has rather peaked profiles and its value is relatively large. When the plasma is located in the strong field region far from the wall with large a , σ_i is small and has rather flat distribution.²⁹ We measured local image charge density at different walls by using analog integration circuits

$$\sigma_i = I_i dt / S \quad (4)$$

and tried to reconstruct the spatial plasma profiles. Here I_i is the image current and S is the area of a wall probe facing the plasma. Figure 6 shows the temporal evolution of the estimated plasma shape. The averaged confinement region temporally shifts inward to strong field region. During beam injection, plasma filled approximately the entire region inside the magnetic separatrix. After beam injection ended, electrons whose orbits are intersecting the electron gun structure are lost, and the plasma mainly distributed in a strong field region near the superconducting magnet. The peaked density profile was stably sustained until the end of the confinement at $t = 320$ s.

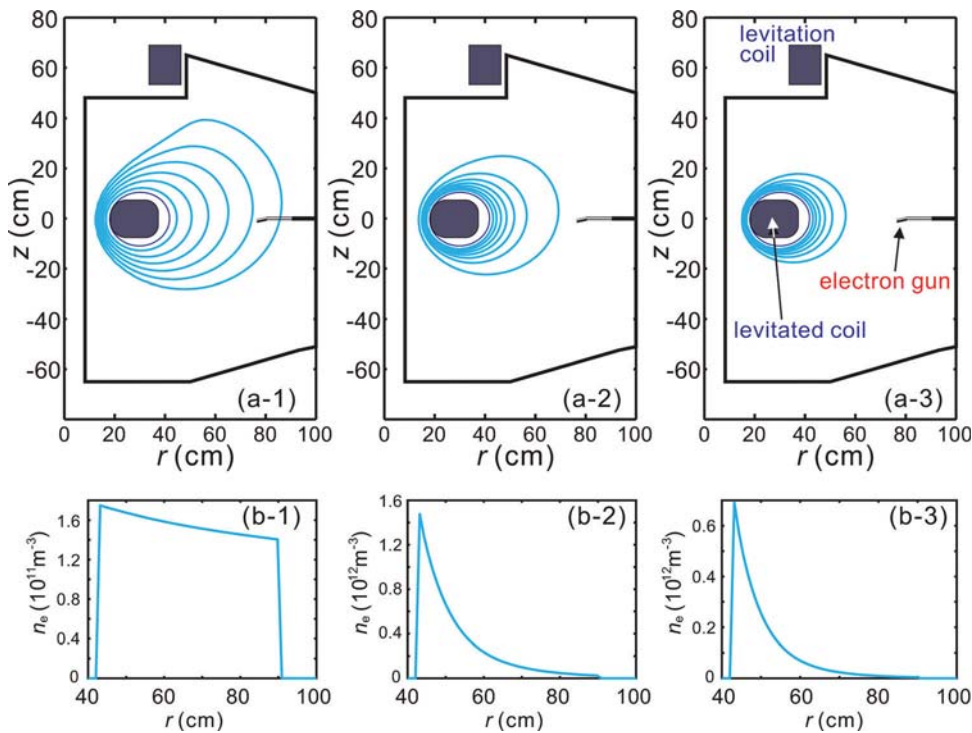


FIG. 6. (Color online) Reconstructed density profiles of non-neutral plasma based on wall probe measurements (Ref. 29). (a) Contours and (b) radial profile on $z=0$ plane of density profiles (1) during beam injection, (2) just after injection ended, and (3) just before confinement ended. Best fitting was obtained when a in Eq. (3) was (1) 0.3, (2) 5.6, and (3) 7.0.

IV. FORMATION OF HIGH- β ECH PLASMA

A. Magnetospheric high temperature plasma

The main purpose of the RT-1 device is the realization of stable confinement of high- β plasma suitable for advanced fusion concept. In magnetospheric plasma, the effects of flow and strongly inhomogeneous field play important roles in the confinement and stability properties. The mechanism of high- β equilibrium is theoretically explained by the hydrodynamic pressure of fast flow (double Beltrami state).^{10,11} Study of high- β flowing plasma is important for understanding the fundamental physics of self-organization of magnetized charged particles as well as for the realization of advanced fusion. In ECH plasma experiment carried out so far, low density ($\sim 10^{17} \text{ m}^{-3}$) and high temperature ($\sim 10 \text{ keV}$) hot electron plasma has been generated. In this parameter regime, ion inertia length ($\sim 1 \text{ m}$) is longer than the scale length of the plasma, and diversity of plasma structures emerged by two-fluid effects can be studied.⁶ In this section, recent results of the high- β plasma experiment in RT-1 are explained.

B. Formation of high- β plasma

After the first plasma in 2006, we have conducted optimization of plasma formation conditions in RT-1 and realized drastic improvement of the plasma performance.²⁴ The optimization includes the realization of stable magnet levitation, installation of multifrequency (8.2 and 2.45 GHz) microwaves for ECH, and the construction of geomagnetic field compensation coils.²⁷ Figure 7 shows a visible light image and soft x-ray images of the plasma observed by a CCD camera.³⁰ As shown in Fig. 7(a), the support structure for the superconducting magnet is a serious loss route of hot electrons and strong bremsstrahlung is observed on it when the superconducting magnet is not levitated. Improvements in both stored magnetic energy and line integrated density are realized by the magnet levitation. For high β plasma, the magnetic separatrix expands outward due to the increased toroidal diamagnetic current. In such cases, some hot electrons hit the chamber wall and are lost there, as shown in Fig. 7(b). Figure 8 shows the effects of the insertion of a limiter at the edge confinement region. For the measurements of bremsstrahlung x-ray, Si(Li) detectors were installed at vertical ports at $r = 60$ and 72 cm with pulse height analysis

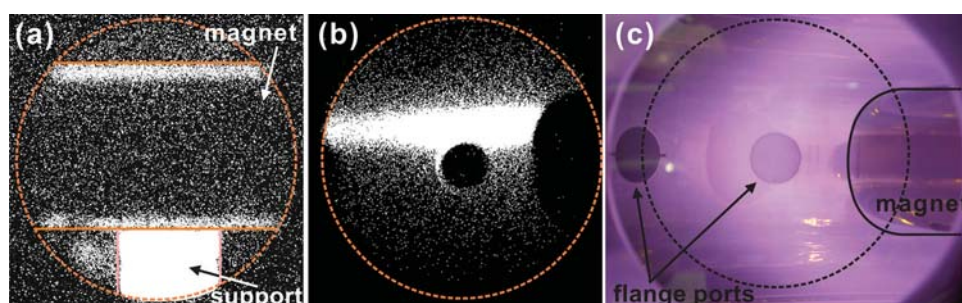


FIG. 7. (Color online) (a) x-ray image of plasma, superconducting magnet, and support structure (Ref. 30). (b) X-ray image and (c) visible light image from tangential port for high- β plasma.

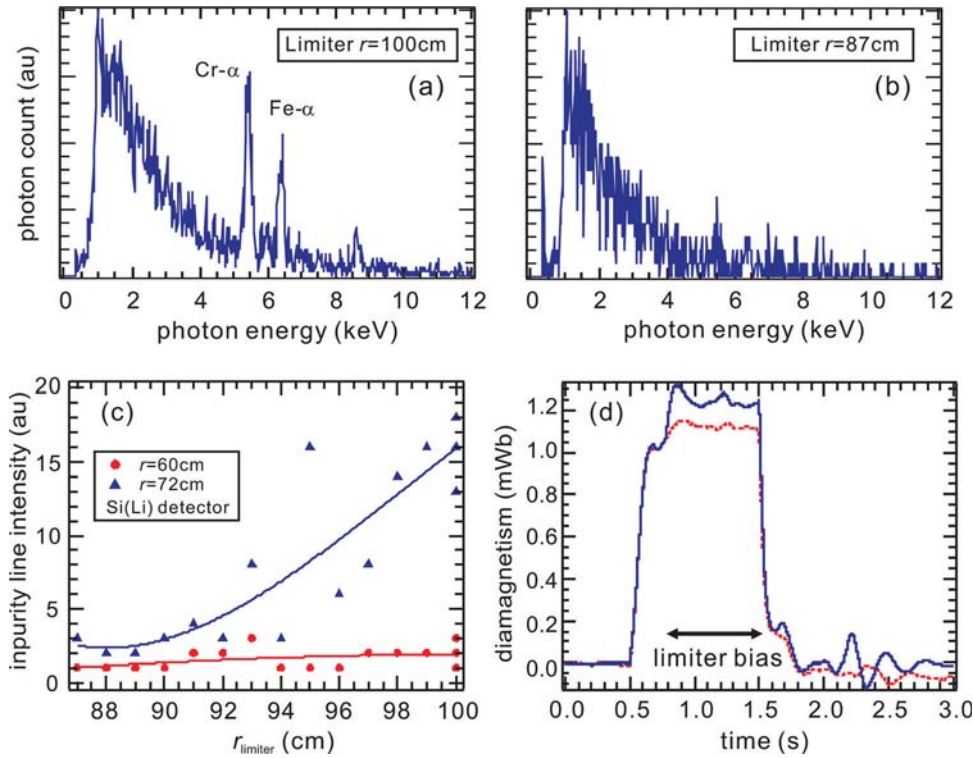


FIG. 8. (Color online) Typical PHA data of x-ray photons (a) when limiter was located outside of separatrix and (b) when located at edge of confinement region. (c) Impurity line strength observed at $r = 62$ and 72 cm cords in variation of horizontal limiter position. (d) Diamagnetic signal with (solid line) and without (dotted line) positive bias on limiter.

(PHA) systems. When a limiter (molybdenum block) was located just inside the magnetic separatrix in Fig. 8(b), x-ray line intensities of Fe and Cr impurities are drastically reduced when compared with a case without limiter insertion [Fig. 8(a)]. Impurity lines were evident at plasma edge region rather than the central region, as shown in Fig. 8(c), indicating that the impurities were caused by the spattering of the SUS304 stainless-steel chamber wall. Figure 8(d) shows the effects of limiter bias. When the limiter was biased to +1 kV, typically 10 % of increase in the diamagnetic signal was observed, suggesting the enhanced confinement of electrons.

Plasma in high- β states is generated depending on the filled neutral gas pressure P_n and injected microwave power P_f . The highest electron density is realized at $P_n > 4$ mPa, but plasma pressure is rather low in this pressure range. High β plasma is realized in a pressure range of 0.4–4 mPa. When P_n is lower than ~ 0.4 mPa, plasma becomes unstable and it

has rather low diamagnetic pressure and density. In ECH experiments in RT-1 carried out so far, plasma pressure mainly resulted from hot electrons, and the highest β is realized by increasing the input RF power and lowering P_n close to the unstable range.

Temporal evolutions of plasma for the cases of low and high β states are shown in Fig. 9. Diamagnetic signal of the plasma is measured by four magnetic loops winded outside of the chamber. Equilibrium pressure profiles of the plasma are calculated by using two dimensional Grad-Shafranov analysis based on the magnetic measurements. There is an empirical relation between the averaged diamagnetic loop signal $\Delta\Psi$ and the maximum local β : β (%) $\sim 18 \times \Delta\Psi$ (mWb) in the present plasma pressure range. The high- β plasma [Fig. 9(b)] was generated with applied microwave power of 20 kW at 2.45 GHz and 25 kW at 8.2 GHz both injected from $t = 0$ to 1 s at $P_n = 0.5$ mPa and is characterized by large stored energy, strong x-ray radiation, and

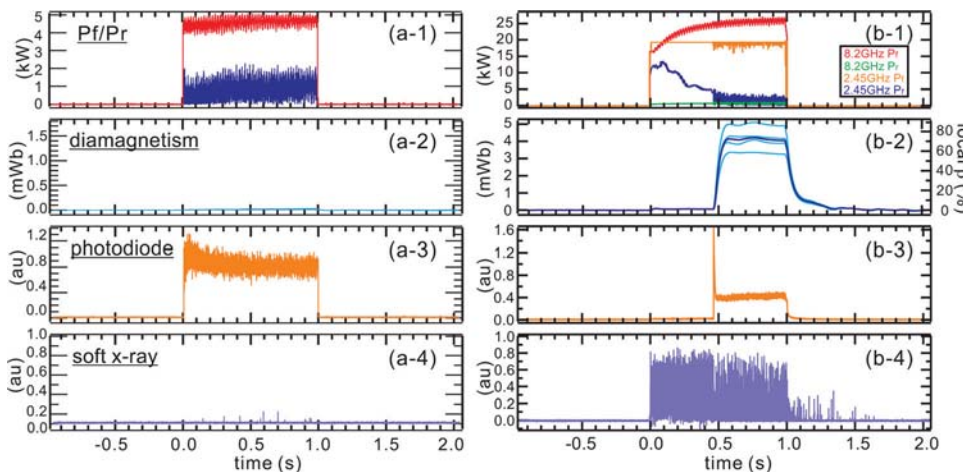


FIG. 9. (Color online) Typical wave-forms of (a) low power and (b) high power plasma formation. (1) Injection and reflection microwave powers, (2) diamagnetic loop signals and corresponding local β , (3) visible light strength, and (4) soft x-ray signal.

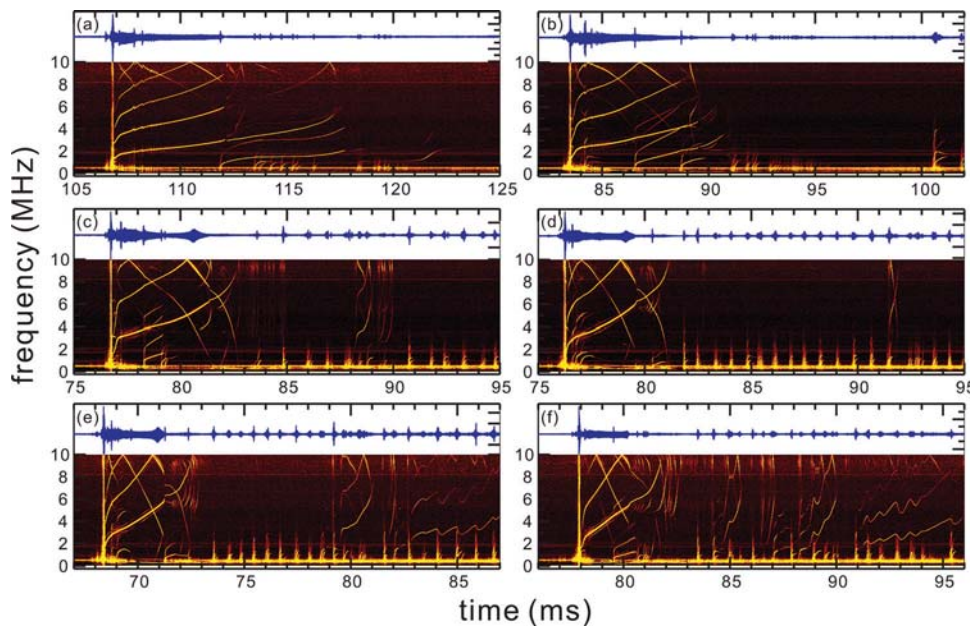


FIG. 10. (Color online) Temporal evolutions of magnetic fluctuation and frequency power spectrum observed in low density and high temperature state. Injected 2.45 GHz microwave power was (a) 2.5 kW, (b) 5 kW, (c) 9 kW, (d) 12 kW, (e) 17 kW, and (f) 19 kW.

depression of visible light strength. At this neutral gas pressure, there is a time lag between the start of microwave injection and high density plasma formation. From $t = 0$ to 0.46 s, very low density (typically $\sim 10^{15} \text{ m}^{-3}$) plasma was generated with strong x-ray radiation, suggesting that thin plasma consists of extremely hot electrons. The reflection power gradually decreased during continuous microwave injection, and jump to a high density state was observed at $t = 0.46$ s accompanied with a rapid increase in visible light strength. Then, the strength of visible light dropped rapidly and the stored energy started to increase. After the increase in stored energy, saturated high β stable state was realized. In the data shot presented in Fig. 9(b), the maximum local β is calculated to be 70%, and the pressure peak was located at $r = 49$ cm on the $z = 0$ cm plane. The plasma had a typical density of $\sim 10^{17} \text{ m}^{-3}$ in this phase. After microwaves were turned off at $t = 1$ s, plasma density and diamagnetic signal decayed slowly.

During the initial phase of microwave injection in Fig. 9(b), high density state is not realized and the plasma has electromagnetic fluctuations. Figure 10 shows temporal evolution of magnetic fluctuation and its frequency power spectrum measured by a pickup coil. The magnetic fluctuation level was $\sim 10^{-5}$ T. After the onset of instability, chirping of frequency was observed. The frequency sweep rate is correlated with conditions of plasma formation, and faster chirp was observed by increasing P_f as shown in the figure. High frequency fluctuations have also been observed in Collisionless Terrella Experiment (CTX) (Refs. 31–33) and LDX,³⁴ and the effects of hot electrons are possible reasons for the observed onset of instability.

C. Confinement time and spatial profile of plasma

Soft x-ray measurements using Si(Li) detectors show that the hot electron component is in the temperature range of up to ~ 50 keV. Edge Langmuir probe measurements show that plasma also has cold electrons around 10 eV. The

hot electron component has relatively long confinement time due to its small cross section of neutral collisions. Decay curve of line density has two different time constants, corresponding to the hot and cold components of electrons. By optimizing neutral gas pressure, the ratio of hot component reached 60%.²⁴ Confinement time of the hot electrons is primarily decided by the neutral gas pressure, and $\tau_p = 0.5$ s at $P_n = 8 \times 10^{-4}$ Pa as shown in Fig. 11(a). Energy confinement time $\tau_E \sim 50$ ms during microwave injection [Fig. 11(b)], estimated from P_f and P_r of microwaves, and the stored energy of plasma, is shorter than τ_p , partially because

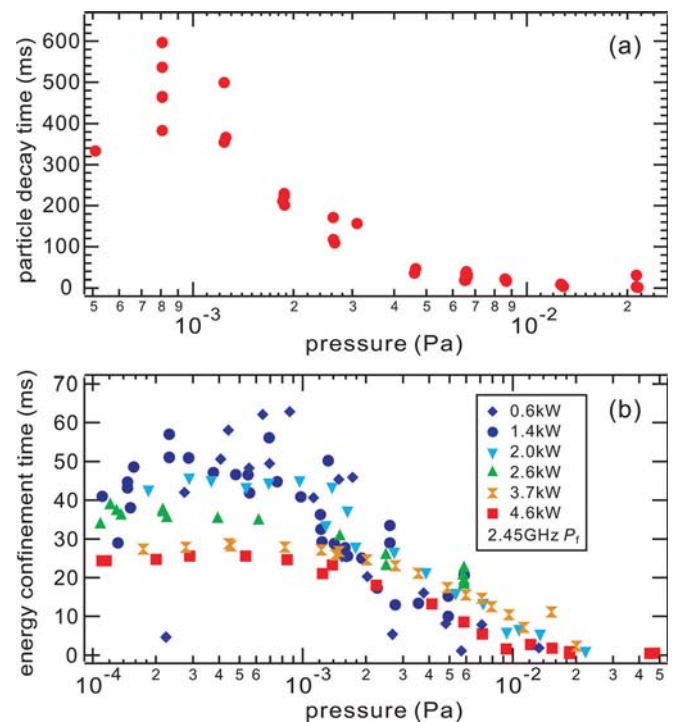


FIG. 11. (Color online) (a) Time constants of slow decay component of interferometer signal after microwave injection ended (Ref. 24). (b) Energy confinement time estimated from stored energy and injected microwave power.

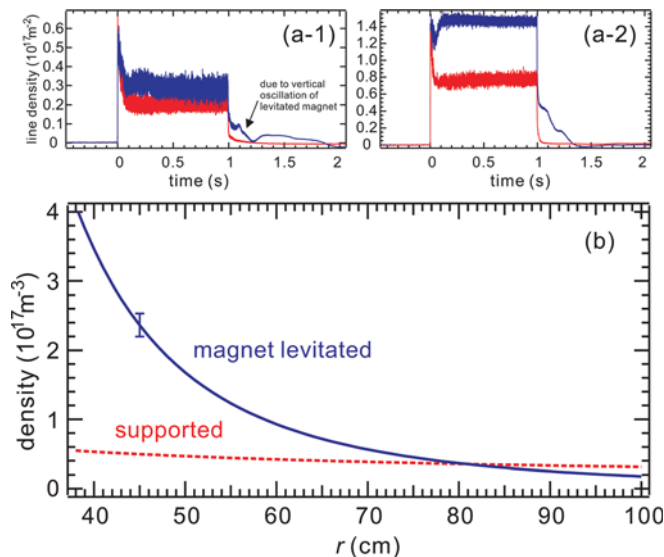


FIG. 12. (Color online) (a) Interferometer signals when the magnet was not levitated (dotted lines) and levitated (solid lines), measured at (1) vertical cord at $r = 72 \text{ cm}$ and (2) tangential cord at $y = 45 \text{ cm}$. (b) Density profiles inferred from multicord interferometry with and without magnet levitation (Ref. 24).

of the effects of low temperature electrons and absorption efficient of the microwave power to the plasma. More accurate measurements of τ_E and its spatial properties using fast magnetic probes will be presented elsewhere.

Plasma density profiles were estimated by using multicord interferometry, again assuming that the electron density has power-low dependence on r on the $z = 0$ plane, as shown in Eq. (3), and is constant on magnetic surfaces. Figure 12 shows the radial density profiles when $P_f = 16 \text{ kW}$ with and without coil levitation. By removing perturbations due to the coil support structure, peaked density profile is realized.^{5,24} A drastic increase in the density was observed in the measurement of the interferometer at the tangential cord [Figs. 12(a) and 13], indicating the increase in density in a strong field region. The best fit was obtained for $a = -0.3$ when the coil was not levitated, and $a = 2.8$ when levitated. When P_f is small, we measured the electron density also by using an edge Langmuir probe and found

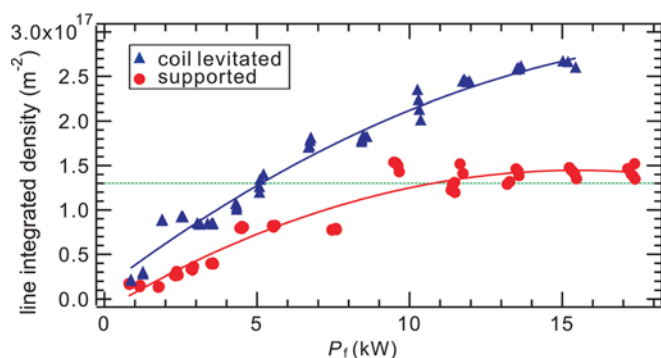


FIG. 13. (Color online) Line density n_l of electrons measured at tangential ports in variation of 2.45 GHz microwave power with and without magnet levitation. Dotted line shows n_l when averaged density on interferometer path is equal to 2.45 GHz cutoff density.

that it was consistent with the estimation from multicord interferometer measurements.

V. SUMMARY

We reported the recent experimental progress of the magnetospheric plasmas in RT-1. In toroidal non-neutral plasma experiment, pure electron plasma was stably trapped for more than 300 s. Spatial structures and fluctuation properties indicate the self-organization of toroidal rigid-rotating equilibrium state. Onset of instability induces asymmetry of the trap system, and effective inward diffusion and density increase were observed in the strong field region. For high- β ECH plasma experiment, maximum local β value has reached 70%, and electrons consist of a majority of hot component and the rest of cold component. High- β state is realized by avoiding the electromagnetic fluctuations. The plasma has peaked density profiles in the strong field region, which is consistent with the prediction of Hasegawa,⁸ that turbulent-induced diffusion occurs so that peaked plasma density is generated in the strong field region.

ACKNOWLEDGMENTS

This work was supported by Grants-in-Aid for Scientific Research (14102033 and 19340170) from MEXT, Japan.

- ¹Z. Yoshida, Y. Ogawa, J. Morikawa, S. Watanabe, Y. Yano, S. Mizumaki, T. Tosaka, Y. Ohtani, A. Hayakawa, and M. Shibui, *J. Plasma Fusion Res.* **1**, 008 (2006).
- ²Y. Ogawa, Z. Yoshida, J. Morikawa, H. Saitoh, S. Watanabe, Y. Yano, S. Mizumaki, and T. Tosaka, *J. Plasma Fusion Res.* **4**, 020 (2009).
- ³Z. Yoshida, H. Saitoh, J. Morikawa, Y. Yano, S. Watanabe, and Y. Ogawa, *Phys. Rev. Lett.* **104**, 235004 (2010).
- ⁴D. T. Garnier, A. K. Hansen, J. Kesner, M. E. Mauel, P. C. Michael, J. V. Minervini, A. Radovinsky, A. Zhukovsky, A. Boxer, J. L. Ellsworth, I. Karim, and E. E. Ortiz, *Fusion Eng. Des.* **81**, 2371 (2006).
- ⁵A. C. Boxer, R. Bergmann, J. L. Ellsworth, D. T. Garnier, J. Kesner, M. E. Mauel, and P. Woskov, *Nature (London), Phys. Sci.* **6**, 207 (2010).
- ⁶Z. Yoshida, S. M. Mahajan, T. Mizushima, Y. Yano, H. Saitoh, and J. Morikawa, *Phys. Plasmas* **17**, 112507 (2010).
- ⁷S. M. Krimigis, T. P. Armstrong, W. I. Axford, C. O. Bostrom, C. Y. Fan, G. Gloeckler, L. J. Lanzerotti, E. P. Keath, R. F. Zwickl, J. F. Carbarry, and D. C. Hamilton, *Science* **206**, 977 (1979).
- ⁸A. Hasegawa, *Comments Plasma Phys. Controlled Fusion* **11**, 147 (1987).
- ⁹J. Kesner, D. T. Garnier, A. Hansen, M. Mauel, and L. Bromberg, *Nucl. Fusion* **44**, 193 (2004).
- ¹⁰S. M. Mahajan and Z. Yoshida, *Phys. Rev. Lett.* **81**, 4863 (1998).
- ¹¹Z. Yoshida and S. M. Mahajan, *Phys. Rev. Lett.* **88**, 095001 (2002).
- ¹²A. Hasegawa, L. Chen, and M. E. Mauel, *Nucl. Fusion* **30**, 2405 (1990).
- ¹³M. Schulz and L. J. Lanzerotti, *Particle Diffusion in the Radiation Belts* (Springer, New York, 1974).
- ¹⁴R. C. Davidson, *Physics of Nonneutral Plasmas* (Imperial College Press, London, 2001).
- ¹⁵J. D. Daugherty, J. E.ninger, and G. S. Janes, *Phys. Fluids* **12**, 2677 (1969).
- ¹⁶P. Zaveri, P. I. John, K. Avinash, and P. K. Kaw, *Phys. Rev. Lett.* **68**, 3295 (1992).
- ¹⁷Z. Yoshida, Y. Ogawa, J. Morikawa, H. Himura, S. Kondoh, C. Nakashima, S. Kakuno, M. Iqbal, F. Volponi, N. Shibayama, and S. Tahara, in *Non-Neutral Plasma Physics III*, AIP Conf. Proc. (AIP, New York, 1999), Vol. 498.
- ¹⁸H. Saitoh, Z. Yoshida, C. Nakashima, H. Himura, J. Morikawa, and M. Fukao, *Phys. Rev. Lett.* **92**, 255005 (2004).
- ¹⁹J. P. Marler and M. R. Stoneking, *Phys. Rev. Lett.* **100**, 155001 (2008).
- ²⁰S. Pahari, H. S. Ramachandran, and P. I. John, *Phys. Plasmas* **13**, 092111 (2006).

- ²¹H. Himura, H. Wakabayashi, Y. Yamamoto, M. Isobe, S. Okamura, K. Mat-suoka, A. Sanpei, and S. Masamune, *Phys. Plasmas* **14**, 022507 (2007).
- ²²J. P. Kremer, T. S. Pedersen, R. G. Lefrancois, and Q. Marksteiner, *Phys. Rev. Lett.* **97**, 095003 (2006).
- ²³H. Saitoh, Z. Yoshida, J. Morikawa, Y. Yano, H. Hayashi, T. Mizushima, Y. Kawai, M. Kobayashi, and H. Mikami, *Phys. Plasmas*, **17**, 112111 (2010).
- ²⁴H. Saitoh, Z. Yoshida, J. Morikawa, Y. Yano, T. Mizushima, Y. Ogawa, M. Furukawa, K. Harima, Y. Kawazura, K. Tadachi, S. Emoto, M. Kobayashi, T. Sugiura, G. Vogel, in Proceedings of the 23rd IAEA Fusion Energy Conference EXC/9-4Rb (2010).
- ²⁵S. Mizumaki, T. Tosaka, Y. Ohtani, M. Ono, T. Kuriyama, K. Nakamoto, M. Shibui, N. Tachikawa, S. Ioka, J. Morikawa, Y. Ogawa, Z. Yoshida, *IEEE Trans. Appl. Supercond.* **16**, 918 (2006).
- ²⁶Y. Yano, Z. Yoshida, Y. Ogawa, J. Morikawa, and H. Saitoh, *Fusion Eng. Des.* **85**, 641 (2010).
- ²⁷Y. Yano, Z. Yoshida, J. Morikawa, H. Saitoh, H. Hayashi, and T. Mizush-ima, *Plasma Fusion Res.* **4**, 039 (2009).
- ²⁸C. Nakashima, Z. Yoshida, H. Himura, M. Fukao, J. Morikawa, and H. Saitoh, *Phys. Rev. E* **65**, 036409 (2002).
- ²⁹H. Saitoh, Y. Yano, T. Mizushima, J. Morikawa, and Z. Yoshida, *Plasma Fusion Res.* **4**, 054 (2009).
- ³⁰H. Saitoh, Y. Yano, T. Mizushima, J. Morikawa, and Z. Yoshida, *Plasma Fusion Res.* **4**, 050 (2009).
- ³¹H. P. Warren, M. E. Mael, D. Brennan, and S. Taromina, *Phys. Plasmas* **3**, 2143 (1996).
- ³²B. Levitt, D. Maslovsky, and M. E. Mael, *Phys. Plasmas* **9**, 2507 (2002).
- ³³D. Maslovsky, B. Levitt, and M. E. Mael, *Phys. Rev. Lett.* **90**, 185001 (2003).
- ³⁴D. T. Garnier, A. Hansen, M. E. Mael, and E. Ortiz, A. Boxer, J. Ells-worth, I. Karim, J. Kesner, S. Mahar, and A. Roach, *Phys. Plasmas* **13**, 056111 (2006).